The strategy for coupling the RanGTP gradient to nuclear protein export

Attila Becskei* and Iain W. Mattaj†

Gene Expression Programme, European Molecular Biology Laboratory, D-69117 Heidelberg, Germany

Communicated by Fotis C. Kafatos, European Molecular Biology Laboratory, Heidelberg, Germany, December 17, 2002 (received for review August 12, 2002)

The Ran GTPase plays critical roles in both providing energy for and determining the directionality of nucleocytoplasmic transport. The mechanism that couples the RanGTP gradient to nuclear protein export will determine the rate of and limits to accumulation of export cargoes in the cytoplasm, but is presently unknown. We reasoned that plausible coupling mechanisms could be distinguished by comparing the rates of reverse motion of export cargoes through the nuclear pore complex (NPC) with the predictions of a mathematical model. Measurement of reverse export rates in *Xenopus* oocytes revealed that nuclear export signals can facilitate RanGTP-dependent cargo movement into the nucleus against the RanGTP gradient at rates comparable to export rates. Although export cargoes with high affinity for their receptor are exported faster than those with low affinity, their reverse transport is also greater. The ratio of the rates of reverse and forward export of a cargo is proportional to its rate of diffusion through the NPC, i.e., to the ability of the cargo to penetrate the NPC permeability barrier. The data substantiate a diffusional mechanism of coupling and suggest the existence of a high concentration of RanGTP-receptor complexes within the NPC that decreases sharply at the cytoplasmic boundary of the NPC permeability barrier.

Transport of macromolecules between the nucleus and cytoplasm (1, 2) is generally an active, receptor-mediated process. A large majority of characterized transport events involve members of the importin β family of import and export receptors. The Ran GTPase, in its GTP state, binds to these receptors and regulates their interaction with cargos in a compartment-specific manner. Transport across the nuclear envelope (NE) occurs through nuclear pore complexes (NPCs), large proteinaceous structures that penetrate the NE and form aqueous channels. NPCs act as permeability barriers through which specific cargos are translocated by transport receptor-mediated facilitated diffusion.

Proteins containing a leucine-rich nuclear export signal (NES) form an export complex in the nucleus by binding cooperatively with RanGTP to the export receptor CRM1 (1–5). On translocation through the NPC, export complexes are generally dissociated by the action of RanBP1 or RanBP2 and RanGAP in the cytoplasm, which together induce Ran to hydrolyze bound GTP and thus render export complex dissociation irreversible (1, 2, 6–8). For the completion of a nuclear export cycle, RanGDP is reimported into the nucleus (9, 10) and the bound GDP is exchanged to GTP by Ran's guanosine nucleotide exchange factor, RCC1. The reactions mediated by nuclear RCC1 and cytoplasmic RanGAP generate a gradient of RanGTP concentration across the NPC (11), which in turn, because of its influence on export receptor–cargo interactions, drives the vectorial movement of export cargoes. A similar logic applies to all known Ran-dependent nucleocytoplasmic transport events (1, 2). Despite the identification of the components of the export machinery and the insight into their functions described above, a fundamental aspect of export remains unresolved: how the RanGTP gradient is coupled to cargo transport. In other words, how efficiently the energy released by hydrolysis of RanGTP is converted into an asymmetric distribution across the NPC of RanGTP-dependent export cargoes. In principle, the mechanism of coupling can influence both the steady-state cellular distribution of export cargoes and the rate of export complex translocation.

Facilitated transport between two compartments mediated by mobile carriers can only be efficient if dissociation of the ligand-carrier complex occurs within a short distance of the boundary of the target compartment (12, 13). In the case of nuclear export, the export complex dissociation and GTP hydrolysis reactions can theoretically occur in an extended space around the NPC. The efficiency of nuclear export is expected to be reduced if the RanGTP concentration decreases gradually on the cytoplasmic side of the NPC, even at a fixed ratio of nuclear and cytoplasmic RanGTP concentration. In addition, temporal changes in the rate of energy supply in the form of ATP or GTP might influence the efficiency of coupling (14–16).

In principle, the translocation of export complexes through the asymmetrically structured NPC could be achieved either by unidirectional movement or by random diffusion, and variants of both NPC translocation mechanisms have been proposed (8, 17–23). Although the rate of translocation can be accelerated by the presence of rectified steps in diffusion, random diffusion in asymmetric structures can only be converted into unidirectional movement if it is coupled to a nonequilibrium reaction (16, 24). There are mechanisms by which the energy of interaction between proteins can be transduced into directed motion that do not depend on nucleotide hydrolysis, but these usually operate over very limited distances (25). A comparison of *in vivo* translocation rates in both directions across the NPC would shed light on the presence of either randomness or biased motion during NPC translocation. *In vitro* studies that manipulated the RanGTP gradient have demonstrated that export complexes can move into the nucleus if RanGTP hydrolysis in the cytoplasm is prevented (21). To understand the mechanism of coupling, however, it is crucial to examine the process under *in vivo* conditions in which both the synergy of all (e.g., refs. 26 and 27) factors relevant for the export process and the natural flux rates of the reactions of the RanGTP cycle are preserved (14–16).

We reasoned that it would be possible to analyze the effects of the RanGTP gradient and directional diffusion of export complexes within the NPC if the export process was decomposed into two opposing directions of Brownian motion and therefore measured the movement of export cargoes into the nucleus under various conditions. In parallel, the reaction-diffusion process underpinning nuclear export was analyzed with the help of equations representing aspects of the transport process derived from a general mathematical model. The first equation establishes that the ratio of reverse and forward export is inversely proportional to the steepness of the cytoplasmic part of the RanGTP gradient. The second equation shows that the portion of the gradient within the NPC can facilitate reverse export in direct, linear proportion to the passive diffusion rate of

Abbreviations: NPC, nuclear pore complex; NES, nuclear export signal; DHFR, dihydrofolate reductase.

*Present address: Department of Physics, 13-2009, Massachusetts Institute of Technology, Cambridge, MA 02139.

†To whom correspondence should be addressed. E-mail: mattaj@embl-heidelberg.de.

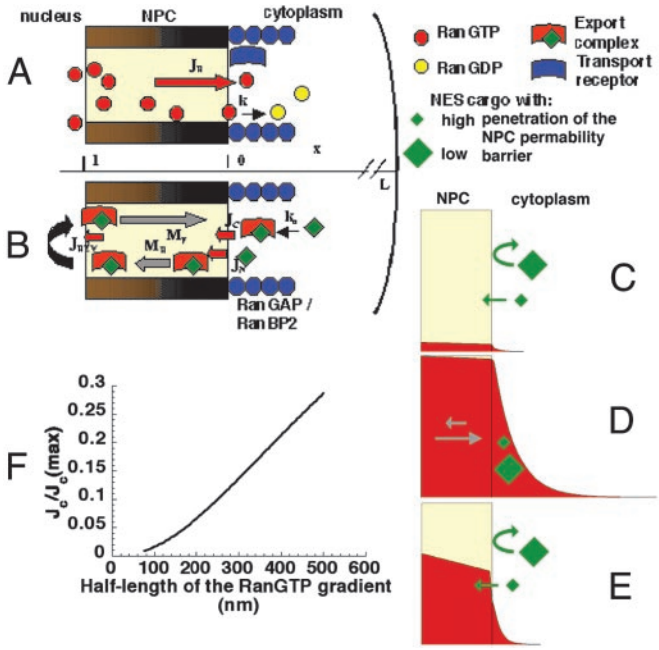

Fig. 1. Models of the RanGTP gradient and its coupling to export. The yellow area within the NPC represents the permeability barrier. RanGTP represents RanGTP-receptor complexes (see text). Note that all of the cartoons are illustrative rather than attempts at literal representation. (*A*) The formation of the RanGTP gradient is primarily determined by the flux of RanGTP (J_R) accessible for export complex formation and the rate of GTP hydrolysis on Ran (k). (*B*) The reverse flux of export complexes (J_{REV}) might arise from their formation either in the cytoplasm (J_C) or, after permeation of export cargoes through the NPC permeability barrier (J_N), within the NPC. Directional motion of export cargoes can be generated within the NPC if there is a mechanism to favor the movement in the forward direction (M_F) at the expense of the reverse direction (M_R). (*C–E*) Models of the shape of the RanGTP gradient (plotted based on Eq. **6**, see *Supporting Methods*) and reverse export in different conditions. Export complexes are formed when cargoes encounter RanGTP and CRM1 (i.e., when they enter the red field on the panels). The permeability of NES cargoes will be affected by both the size and surface properties of the cargo (29). (*C*) J_R is low and k is high. (*D*) J_R is high and k is low. The movement of export cargoes in the NPC is biased in the forward direction (gray arrows). (*E*) J_R is high and k is high and the partitioning of RanGTP into the NPC from the nucleus is intermediate to high. (*F*) In the parametric plot both the normalized rate of complex entry into the NPC [J_C/J_C(max)] and the half-length of the RanGTP gradient is plotted as a function of the RanGTP hydrolysis rate. J_C(max) represents J_C in the absence of RanGTP hydrolysis. The following published parameter values were used for Eqs. **2** and **7**: $D = 5\ \mu m^2 s^{-1}$, $l = 0.04\ \mu m$, $k_n = 10\ s^{-1}$, k_b was varied from 10 to 400 s^{-1} (8, 19, 30, 34).

an export cargo across the NPC. By fitting the experimental data to these equations, it was possible to reconstruct properties of the *in vivo* RanGTP gradient and its coupling to the movement of export cargoes.

Methods

Reaction-Diffusion Model of Coupling. The following model describes the formation of the RanGTP gradient (Fig. 1*A*) and its effect on the reverse motion of export complexes into the NPC (Fig. 1*B*). The modeling approach circumvents the impossibility of exactly solving reaction-diffusion equations which describe facilitated diffusion with mobile carriers (12, 28). The equilibrium concentration of RanGTP (r), usually bound to a transport receptor (see below), NES-containing export cargoes (n), and complexes (c) within the NPC in relation to the rest of the cell is determined by their partition coefficients (K_R, K_N, K_C) (29). The diffusion constant of these components in the cytoplasm is denoted by D. On exit from the NPC with a flux rate J_R, RanGTP. is hydrolyzed at a rate k. The concentration profile of RanGTP (r) at steady state is obtained from the following equation, when the boundary conditions at the cytoplasmic face of the NPC ($x = 0$) and cell membrane ($x = L$) are given in the following way:

$$\frac{\partial r}{\partial t} = D\frac{\partial^2 r}{\partial x^2} - kr \qquad \begin{matrix}\left[\frac{dr}{dx}\right]_{x=0} &=& -\frac{J_R}{K_R D}\\ \left[\frac{dr}{dx}\right]_{x=L\approx\infty} &=& 0\end{matrix} \qquad [1]$$

The normalized flux of export complexes into the NPC from the cytoplasm, J_C/J_C (max), is given by Eq. **2** (for derivation, see *Supporting Methods*, which is published as supporting information on the PNAS web site, www.pnas.org), where k_N is a is a derived first-order constant for the association rate of NES cargoes with CRM1 and RanGTP in the cytoplasm, and l is the length of the diffusion barrier of the NPC.

$$\frac{J_C}{J_C(\max)} = \frac{1 - \sqrt{\frac{k}{k+k_N}}}{l\sqrt{\frac{k}{D}} + 1}. \qquad [2]$$

Free NES cargoes can also enter the NPC at a rate J_N and form export complexes within the NPC with CRM1-RanGTP (the equilibrium chemical activity of CRM1-RanGTP is denoted by r) with a second-order rate constant k_{ON}. The limiting step in this process is the permeation rate of NES cargoes into the NPC because the flux of transport complexes through the NPC is generally significantly higher than that of the free transport cargoes (19). Facilitated export can be described by the following process.

$$\frac{\partial n}{\partial t} = D_{NPC}\frac{\partial^2 n}{\partial x^2} - k_{ON} r n \qquad \begin{matrix}\left[\frac{dn}{dx}\right]_{x=0} &=& -P_N(n_C - n)\\ \left[\frac{dn}{dx}\right]_{x=1} &=& 0\end{matrix}$$

[3]

P_N is a proportionality constant and is characteristic of the rate of the penetration of a free cargo into the NPC. D_{NPC} is the diffusion constant for export cargoes within the NPC and n_C is the cytoplasmic concentration of NES cargoes. The approximate steady-state solution of this equation is

$$J_N \approx D_{NPC} n_C \frac{\lambda P_N}{\lambda + P_N} \qquad \lambda = \sqrt{\frac{k_{ON} r}{D_{NPC}}}. \qquad [4]$$

The facilitation shows a linear dependence on P_N and reaches a plateau at high values of P_N. The entry of free NES cargos into the NPC is increased because of their rapid conversion into complexes with their export receptor.

The two possible sources of reverse flux can be summed

$$J_{REV} = J_C + J_N. \qquad [5]$$

The contribution of J_C to J_{REV} can be determined because only J_N depends on the permeability properties of the export cargo (K_N and D_N). When J_{REV} is plotted against the permeation rate of export cargoes through the NPC in the absence of facilitated diffusion, J_C behaves as a constant and the extrapolated value of J_{REV} at zero permeability equals J_C. J_{REV} has to be normalized by the rate of forward export, so that it becomes independent of

the permeability and diffusion constants of the export complex (see Fig. 4). In summary, J_C reflects the steepness of the RanGTP gradient outside the permeability barrier of the NPC, whereas J_N is determined by the ability of an export cargo to permeate into the NPC and gain access to RanGTP there.

Radioactive Labeling of Recombinant Proteins and Oocyte Injections. Cloning, purification and biotinylation of recombinant proteins are described in *Supporting Methods*. GST protein constructs with an HMK site were labeled in HMK buffer (20 mM Tris·HCl, pH 7.4/100 mM NaCl/12 mM $MgCl_2$). Protein solution (10 μM) was incubated with 25 units of HMK and 50 μCi of [γ-^{35}S]ATP (1 Ci = 37 GBq) for 60 min at room temperature. For nuclear injections, dextran-blue M.W. 2,000,000 was used as a marker and streptavidin, NES constructs, and b-zz-GST were injected at 50, 3, and 75 μM, respectively. For cytoplasmic injections streptavidin, NES constructs, and b-zz-GST were injected at 150, 10, and 75 μM, respectively.

Results

We derived a set of simple equations from the reaction-diffusion equations underpinning nuclear export (see *Methods*) and considered three plausible scenarios for the coupling of nuclear export to the RanGTP cycle based on these equations (Fig. 1). The models were constructed based on the variation of three major parameters: the concentration of RanGTP within the NPC, the slope of the RanGTP gradient in the cytoplasm, and the directionality of export cargo movement within the NPC. Experiments were designed in such a way that their outcome would differentiate between possible coupling mechanisms and reveal which underlies nuclear export. Although we refer to the RanGTP gradient throughout the paper, this is a simplification. Given that most transport receptors examined have been found to be more concentrated in the NPC than elsewhere, and that free RanGTP in the NPC would dissociate incoming import complexes and thus inhibit nuclear import, it is reasonable to assume that we are dealing with RanGTP-receptor complexes rather than free RanGTP. This assumption does not alter our conclusions.

The first model has a low concentration of RanGTP (red) within the NPC and a steep gradient (Fig. 1*C*). A NES cargo would permeate the NPC from the cytoplasm according to its diffusion constant and partition coefficient into the NPC and RanGTP dependent facilitated reverse export would not be detected.

In the second model, the RanGTP level in the perinuclear cytoplasm is high because of a higher concentration of RanGTP in the NPC and slower cytoplasmic hydrolysis (Fig. 1*D*). Because of the high probability of export complex formation in the cytoplasm, a large flux of reverse export would occur. To provide a realistic efficiency of directional transport in this model, it has to be assumed that facilitated diffusion within the NPC is directional (gray arrows) such that only a certain fraction of the export complexes entering the NPC from the cytoplasm would reach the nucleoplasm. Eq. **2** shows that the magnitude of the flux of export complexes arising from the cytoplasm (J_c) is sensitive to the slope of the cytoplasmic gradient of RanGTP concentration (Fig. 1*F*). For example, the rate of reverse export increases 4-fold when the distance from the NPC permeability barrier to the half-maximal RanGTP concentration increases from 100 to 200 nm. The rate of reverse export would reflect the slope of the cytoplasmic RanGTP gradient and the bias in diffusional movement within the NPC, but should not be related to the diffusion rate of free cargo because the species entering the NPC is likely to be the export complex rather than the cargo.

In the third case, the concentration of RanGTP within the NPC can be high or, as shown, intermediate and the slope of the cytoplasmic gradient is steep (Fig. 1*E*). Export complex formation in the cytoplasm is low. However, once an export cargo permeates the NPC it would have a high probability of forming an export complex whose facilitated diffusion in the NPC is higher than that of the uncomplexed export cargo. The limiting step in reverse export in this case is therefore cargo entry into the NPC. Analyzing this scenario by using the mathematical model shows that facilitated reverse export would be linearly proportional to the rate of diffusion of export cargoes through the NPC, i.e., the ability to penetrate the NPC permeability barrier (see Eq. **4**).

To test which of the models best describes nuclear export, NES cargoes with various export signals were constructed and those with differing diffusion constants were selected. We used export signals from the Rev, An3, and NS2 proteins in order of increasing binding affinity to CRM1 (30). We then measured their unidirectional movement through the NPC in the forward and reverse directions by biotinylating the cargoes, then injecting them either into the nucleus or the cytoplasm of *Xenopus laevis* oocytes, and trapping the fraction that moved to the other compartment with streptavidin.

We first measured the rate of forward export by injecting ^{35}S-thiophosphate labeled biotinylated NS2-GST (b-GST-NS2) into the nucleus of *Xenopus* oocytes whose cytoplasm had been preinjected with streptavidin. Analysis of nuclear (N) and cytoplamic (C) fractions showed that b-GST-NS2 was exported rapidly, with a half-time of 12 min (Fig. 2 *A* and *C*). On exit from the nucleus, the streptavidin and b-GST-NS2 formed oligomers, which were mainly detected at the interface of the stacking and resolving gels (Fig. 2*A*). The passive diffusion of the b-GST-NS2 construct was analyzed by coinjection of RanGAP and RanBP1 into the nucleus to remove nuclear RanGTP (Fig. 2 *B* and *D*). The effectiveness of the treatment was tested by demonstrating the lack of accumulation of nonbiotinylated export cargo in the cytoplasm (ref. 5, Fig. 2*F*). The passive diffusion rate of b-GST-NS2 was roughly 13 times lower than its CRM1-mediated forward export (Fig. 2 *C* and *D* and Table 1).

To demonstrate that biotinylated NES-cargoes would be immobilized in the nucleus in the presence of streptavidin, both streptavidin and b-GST-NS2 were injected into *Xenopus* oocyte nuclei. The b-GST-NES was not detectably exported, even 2 h after injection (Fig. 2*E*). Similar results were obtained for all export cargoes (data not shown). This finding indicates that on binding of streptavidin to b-GST-NES no export can occur. For the efficient trapping of injected b-GST-NES by streptavidin, the concentration of streptavidin injected in the nucleus had to be roughly 50-fold higher than that of the b-GST-NES in the cytoplasm (data not shown). In these conditions, a minor misinjection of streptavidin would result in cross-linking of a considerable proportion of cytoplasmic b-GST-NES. To avoid this, a high concentration of biotinylated *z*-tagged GST (b-zz-GST) was coinjected with the b-GST-NES into the cytoplasm. The b-zz-GST would saturate any cytoplasmic streptavidin, and b-zz-GST itself did not diffuse through the NPC (Fig. 2*G*). To avoid biasing the results, the same high ratio of streptavidin to export cargoes was used to measure forward as well as reverse export.

When b-GST-NS2 was injected into the cytoplasm, no detectable diffusion into the nucleus was observed (Fig. 3*A*). However, if the nuclei were preinjected with streptavidin, a gradual increase of b-GST-NS2 signal inside the nucleus was detected by the formation of oligomers containing b-GST-NS2 and streptavidin (Fig. 3*B*, *Upper* is nuclear, *Lower* is cytoplasmic fraction). Nuclear coinjection of RanGAP/RanBP1 reduced the rate of reverse export 3.5-fold, and this value provided a measure of the passive diffusion rate of the construct (Fig. 3*C*). Comparison of the two rates indicates that the motion of export cargoes can be facilitated in the reverse direction as well as in the forward one. A slightly lower diffusion rate was observed when a mutant form of b-GST-NS2, b-GST-Mut(NS2), in which the large hydrophobic amino acids of the NES were replaced by alanines, was

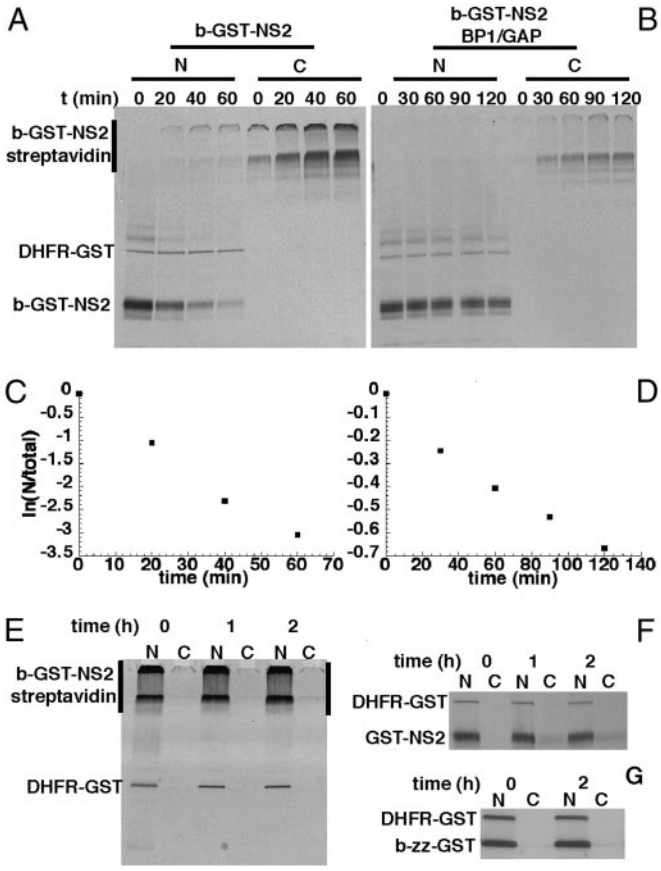

Fig. 2. Forward export measurements and immobilization of NES cargoes by streptavidin. (*A*) Streptavidin (150 μM) was injected into the cytoplasm. After 90 min, a mixture of ^{35}S-thiophosphate-labeled DHFR-GST (nuclear injection control), b-GST-NS2, and unlabeled b-zz-GST was injected into the nucleus. (*B*) The same experiment as in *A*, but the nuclear injection mixture was supplemented by RanGAP and RanBP1 at 200 and 120 μM, respectively. (*C* and *D*) The logarithm of the ratio of the nuclear and total cell signals over time. Note that the ordinate scales are different. The results are presented as first order rates (min^{-1}) in Table 1. (*E*) Injection of streptavidin with b-GST-NS2 and DHFR-GST prevents the export of b-GST-NS2 because of the formation of oligomers. (*F*) Coinjection of RanGAP and RanBP1 efficiently inhibits export of GST-NS2. (*G*) After injection of b-zz-GST into the nucleus no diffusion into the cytoplasm was observed.

injected in the cytoplasm (Fig. 3*D*). However, the diffusion of b-GST-Mut(NS2) from the nucleus was also similarly reduced in comparison to the wild type. This difference is likely to originate from the different surface properties of the two proteins (29). Further evidence for this was obtained by measuring the movement of labeled b-GST-NS2 in the presence of an excess of unlabelled GST-NS2 sufficient to saturate CRM1. In this situation, b-GST-NS2 moved to the cytoplasm at the same rate as in the presence of RanGAP and RanBP1 (data not shown).

Comparison of diffusion rates when b-GST-Mut(NS2) was injected either into the nucleus or into the cytoplasm revealed that the rate of passive diffusion from the cytoplasm to the nucleus was 5.5 times less than in the reverse direction (Fig. 3 *E* and *F*). Similar results were obtained when both b-GST-NS2 and b-GST-An3 were analyzed after nuclear coinjection with RanGAP/RanBP1. This apparent difference reflects the larger volume of the cytoplasm and the resulting partition of export cargoes between the nucleus and cytoplasm. All of the apparent reverse export rates were multiplied by 5.5 to correct for this. The corrected value of the reverse export rate for b-GST-NS2 is therefore $\approx$2.5 times less than the forward rate (Table 1).

To test how the reverse export rate was affected by receptor binding affinity and the ability to permeate the NPC, additional export cargoes were examined. The reverse export rate of b-GST-Rev was 8 times slower than that of b-GST-NS2. However, b-GST-Rev also has a 3-fold reduced forward export rate because of its lower affinity for CRM1 (Table 1). This finding indicates that a higher affinity for CRM1 enhances the flux of an export cargo through the NPC in both directions. In addition, the diffusive passage of b-GST-Rev through the NPC is less than half that of b-GST-NS2, indicating that its penetration of the NPC permeability barrier is reduced, and this accounts for the residual difference between the reverse export rate of the two cargoes.

When b-GST-An3 was injected in the cytoplasm, it showed a reverse export rate comparable to that of b-GST-NS2. Because NS2 has a higher affinity for CRM1 and is also exported approximately two times faster (30), b-GST-An3 would have been expected to have an $\approx$2-fold lower reverse export rate (Table 1). However, by comparison with b-GST-NS2, the b-GST-An3 construct has a passive diffusion rate that is 2-fold higher, and this property counterbalances its lower affinity for CRM1. The reverse export of b-GST-An3 was only reduced 2-fold when RanGAP and RanBP1 were injected into the nucleus (Fig. 3 *G* and *H*, Table 1). When the An3 NES was fused to a dihydrofolate reductase (DHFR)-GST construct, the export rate of b-DHFR-GST-An3 was 2-fold lower than that of b-GST-An3, but its passive diffusion rate dropped >10-fold (Table 1). Accordingly, the reverse export rate dropped below the limit of detection (i.e., >10-fold). This finding indicates that the reverse export rate is highly sensitive to variation in the passive diffusion rate, whereas the export rate is much less so. This can only be explained by a model where the RanGTP gradient on the cytoplasmic side of the NPC permeability barrier is very steep, i.e., the probability of export complex formation in the cytoplasm is very low, such that free cargo needs to permeate into the NPC to encounter CRM1 and RanGTP and form a complex competent for reverse export. For forward export, cargo can encounter RanGTP and CRM1 throughout the accessible nucleoplasm as well as in the

Table 1. Cargo export rates

	Forward rate, min^{-1}	Passive diffusion, min^{-1}	Reverse rate (measured·5.5), min^{-1}	Factor of reduction of reverse rate by GAP/BP1
b-GST-NS2	0.0547 ± 0.0051	0.0052 ± 0.0012	0.0209 ± 0.0040	0.28 ± 0.09
b-GST-An3	0.0243 ± 0.0026	0.0094 ± 0.0017	0.0187 ± 0.0010	0.48 ± 0.12
b-GST-Rev	0.0176 ± 0.0007	0.0020 ± 0.0006	0.0025 ± 0.0003	ND
b-DHFR-GST-An3	0.0140 ± 0.0018	LD	LD	

Average rates were obtained from three measurements after linear fitting of individual measurements like those in Fig. 2 *C* and *D*. The passive diffusion rate was measured by nuclear injection of the respective b-NES-construct in the presence of RanGAP and RanBP1. LD denotes values that are at or below the limit of detection (<0.005 min^{-1}). The rates of slower transport processes cannot be determined accurately because of low signal intensities. ND, not determined. The effect of RanGAP and RanBP1 on reverse export is given.

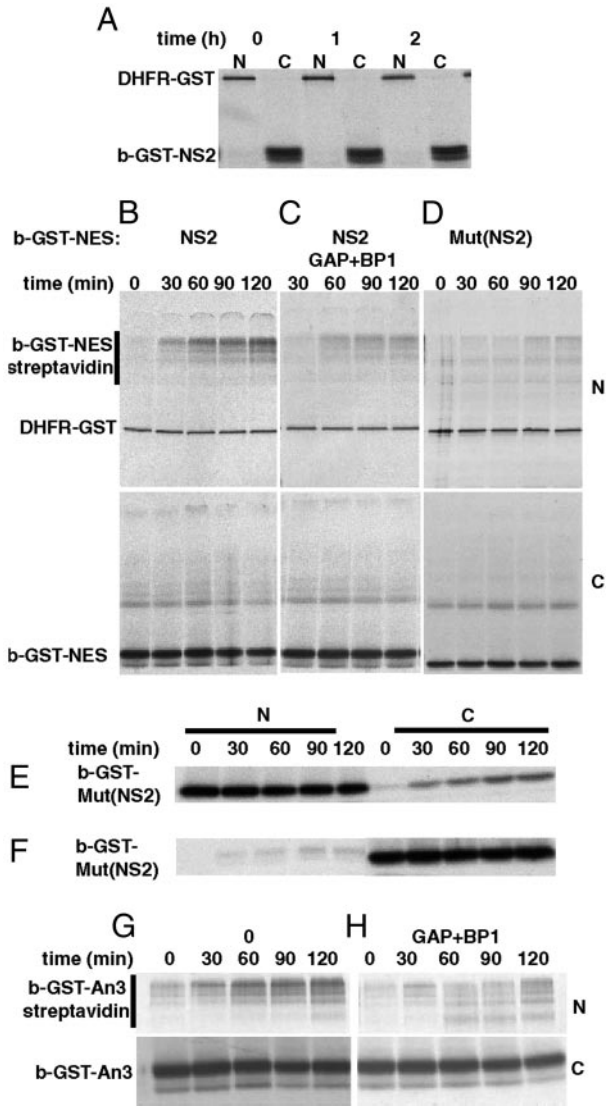

Fig. 3. Reverse export of NES cargoes. (*A*) DHFR-GST was injected into the nucleus. b-GST-NS2 was injected into the cytoplasm 90 min later. Nuclear and cytoplasmic fractions were examined after 0, 1, or 2 h. (*B–D*) DHFR-GST, streptavidin, and, where indicated, RanGAP and RanBP1 were injected into the nucleus. Ninety minutes later, b-GST-NS2 or b-GST Mut (NS2), both supplemented with b-zz-GST, was injected into the cytoplasm. Nuclear and cytoplasmic fractions were examined at the indicated times. (*E*) b-GST and DHFR-GST were injected into the nucleus. (*F*) DHFR-GST was injected into the nucleus and subsequently b-GST-Mut(NS2) was injected into the cytoplasm. (*G*) DHFR-GST and streptavidin were injected into the nucleus. Ninety minutes later, b-GST-An3 supplemented with b-zz-GST was injected into the cytoplasm. (*H*) As in *G*, but RanGAP and RanBP1 were coinjected into the nucleus.

NPC, explaining why the dependence of this process on cargo penetration into the NPC is less.

The generality of the strategy of coupling the RanGTP gradient to nuclear protein export can be analyzed if the ratio between the forward and reverse export rate is plotted against the passive diffusion rate of export cargoes (see Eq. **5**). The use of this ratio corrects for the possibility that the relative rate of movement through the NPC of a complete export complex might depend on the permeability properties of the export cargo present. The data were plotted and shows a linear dependence between the ratio of reverse and forward export rates of export complexes and the passive diffusion rate of the export cargoes involved (Fig. 4). The intersection of the linear fit with the *y* axis

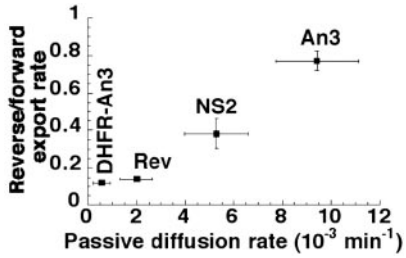

Fig. 4. Dependence of the ratio of reverse and forward export on the passive diffusion rate of export cargoes. DHFR-An3, Rev, An3, and NS2 stand for b-DHFR-An3-GST, b-Rev-GST, b-NS2-GST, and b-An3-GST constructs, respectively. The values are from Table 1. The position of b-DHFR-An3-GST is approximate because the rate of reverse export of this construct is not accurately determined (<0.005 min^{-1}).

is below 0.1, demonstrating that only a small fraction of reverse transport arises from export complexes formed in the cytoplasm, but it cannot be determined exactly as at lower permeation and reverse export rates the signals are too low to be determined accurately.

Discussion

Our results demonstrate, quite unexpectedly, that nuclear export cargoes that have a high rate of diffusion through the NPC permeability barrier can achieve rates of facilitated reverse export *in vivo* that are comparable to their forward export rates. This is remarkable because export complexes moving outward can presumably form in the large accessible volume of the nucleoplasm, whereas our data strongly suggest that those moving in the reverse direction only assemble in the NPC, after movement of free cargo through the permeability barrier. The existence of reverse export will reduce the net rate of export from the nucleus. However, a comparison of the rate of export of the cargoes examined (0.01–0.05 min^{-1}) with the rates of association of RanBP1 and RanGTP or of hydrolysis of RanGTP induced by RanGAP (k_{ass} 10^5–10^6 $M^{-1}{\cdot}s^{-1}$ and k_{cat} 2.1 s^{-1}) (8, 35) shows that the latter processes are more rapid. Therefore, although export complexes containing cargoes with high NPC permeability can translocate toward the nucleus or cytoplasm at similar rates, the fast dissociation and hydrolysis reactions at the cytoplasmic face of the NPC nevertheless generate the observed net cytoplasmic accumulation of export cargoes (Fig. 5).

The linear correlation between passive permeation rates and reverse export rates (Eq. **4**, Fig. 4) substantiates the model of the coupling strategy whereby the cytoplasmic RanGTP gradient is very steep, but there is a relatively high concentration of accessible RanGTP within the NPC (Fig. 1*E*). This facilitates the reverse motion of export cargoes proportionally to their ability to penetrate the NPC permeability barrier by allowing the cargo,

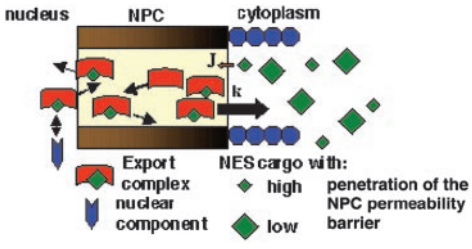

Fig. 5. The model of nuclear protein export. The overall movement of export cargoes does not display directionality in the NPC (arrows with random directions). Export complexes enter the NPC at a slower rate (J) than the rate of RanGTP hydrolysis (k). Export cargoes and complexes with high permeability might interact with nuclear components if they are close enough to the NPC.

once in the NPC, to form an export complex. The fraction of reverse export that originates from cytoplasmic RanGTP, outside of the permeability barrier, is <10% of the forward export rate (Fig. 4). This ratio predicts that the cytoplasmic RanGTP gradient has a half-length of <250 nm (Fig. 1*E*, Eq. **5**).

As discussed in *Results*, RanGTP in the NPC is probably bound to CRM1 and other transport receptors that are concentrated there. The presence of RanGTP in the NPC will reduce the efficiency of coupling in nuclear export below that seen in membrane transport processes. However, imperfection is evident even in coupled membrane transport. For example, during the secondary active transport of glucose, 6–9% of the sodium flux is uncoupled from the flux of glucose (32), lowering the limit to which glucose is accumulated. A 200-fold ratio of nuclear to cytoplasmic RanGTP has been experimentally estimated (11). With perfect coupling, this would lead to a 200-fold greater accumulation of export cargoes in the cytoplasm than in the nucleus, assuming that they are not stably anchored in either compartment. Our results demonstrate that the efficiency of coupling in the nuclear export of different cargoes will be reduced proportionally to their ability to penetrate the permeability barrier of the NPC. Interestingly, it has been shown for coupled membrane transport that the efficiency of coupling can be regulated by either directly affecting the components of the transport machinery itself or by changing the rate of reactions that dissipate energy (33–35). It remains to be determined whether the coupling efficiency and the directionality in movement of nuclear transport complexes can be regulated in a similar way.

In the cases examined here, our data exclude more than a minor role for differential export complex-nucleoporin affinities in generating directional movement across the NPC, and therefore suggest that models for NPC translocation that invoke gradients of binding affinities in generating directionality are unlikely to be correct. The fact remains, however, that there are large differences in the affinity of a given transport receptor for different nucleoporins and that, where examined, high-affinity interactions between nucleoporins and receptors are often affected by RanGTP (8, 18, 36–39). These high-affinity interactions often occur between receptors and nucleoporins that are at the end of the NPC to which the receptor delivers cargo (36, 37, 39) and can greatly influence the efficiency of transport (ref. 40 and references therein). These sites might therefore serve to localize and immobilize transport complexes so that they will be dissociated by the action of the components of Ran cycle before undergoing reverse export or import.

There are possible biological consequences of the fact that reverse export can occur at high rates. The transient appearance of an appropriate export cargo on the nuclear side of the NPC might mediate biochemical or signaling events close to the nuclear face of the NPC (Fig. 5). It has been recently shown that DNA binding protein-transport receptor fusions can localize chromatin domains close to the NPC, and that this localization can alter gene expression (41). Although the overall nuclear concentration of export cargoes subject to reverse export is very low, if the interaction partner of an export cargo were localized close to the nuclear face of NPC it would have a significant probability of interacting with, and having its activity affected by, the export cargo. Such interactions might have an influence on the dynamics of eukaryotic signaling and gene expression networks (42, 43).

We thank P. Askjaer, L. Englmeier, S. Kuersten, A. Segref, and M. Ohno for helpful discussions, and K. Ribbeck, A. van Oudenaarden, and the members of the Mattaj laboratory for criticism of the manuscript. A.B. was supported by the Louis-Jeantet Foundation, and this work was supported in part by the European Molecular Biology Laboratory and the Louis-Jeantet Prize for Medicine (to I.W.M.).

1. Mattaj, I. W. & Englmeier, L. (1998) *Annu. Rev. Biochem*. **67,** 265–306.
2. Gorlich, D. & Kutay, U. (1999) *Annu. Rev. Cell Dev. Biol.* **15,** 607–660.
3. Fornerod, M., Ohno, M., Yoshida, M. & Mattaj, I. W. (1997) *Cell* **90,** 1051–1060.
4. Fukuda, M., Asano, S., Nakamura, T., Adachi, M., Yoshida, M., Yanagida, M. & Nishida, E. (1997) *Nature* **390,** 308–311.
5. Stade, K., Ford, C. S., Guthrie, C. & Weis, K. (1997) *Cell* **90,** 1041–1050.
6. Englmeier, L., Olivo, J. C. & Mattaj, I. W. (1999) *Curr. Biol.* **9,** 30–41.
7. Izaurralde, E., Kutay, U., von Kobbe, C., Mattaj, I. W. & Gorlich, D. (1997) *EMBO J.* **16,** 6535–6547.
8. Kehlenbach, R. H., Dickmanns, A., Kehlenbach, A., Guan, T. & Gerace, L. (1999) *J. Cell Biol.* **145,** 645–657.
9. Ribbeck, K., Lipowsky, G., Kent, H. M., Stewart, M. & Gorlich, D. (1998) *EMBO J.* **17,** 6587–6598.
10. Smith, A., Brownawell, A. & Macara, I. G. (1998) *Curr. Biol.* **8,** 1403–1406.
11. Kalab, P., Weis, K. & Heald, R. (2002) *Science* **295,** 2452–2456.
12. Rubinow, S. I. & Dembo, M. (1977) *Biophys. J*. **18,** 29–42.
13. Scholander, P. F. (1960) *Science* **131,** 585–590.
14. Schell, M., Kundu, K. & Ross, J. (1987) *Proc. Natl. Acad. Sci. USA* **84,** 424–428.
15. Hervagault, J. F., Lazar, J. G. & Ross, J. (1989) *Proc. Natl. Acad. Sci. USA* **86,** 9258–9262.
16. Astumian, R. D. (1997) *Science* **276,** 917–922.
17. Gilchrist, D., Mykytka, B. & Rexach, M. (2002) *J. Biol. Chem.* **277,** 18161–18172.
18. Rexach, M. & Blobel, G. (1995) *Cell* **83,** 683–692.
19. Ribbeck, K. & Gorlich, D. (2001) *EMBO J.* **20,** 1320–1330.
20. Rout, M. P., Aitchison, J. D., Suprapto, A., Hjertaas, K., Zhao, Y. & Chait, B. T. (2000) *J. Cell Biol.* **148,** 635–651.
21. Nachury, M. V. & Weis, K. (1999) *Proc. Natl. Acad. Sci. USA* **96,** 9622–9627.
22. Ben-Efraim, I. & Gerace, L. (2001) *J. Cell Biol.* **152,** 411–417.
23. Koepp, D. M. & Silver, P. A. (1996) *Cell* **87,** 1–4.
24. Astumian, R. D. & Derenyi, I. (1998) *Eur. Biophys. J.* **27,** 474–489.
25. Peskin, C. S., Odell, G. M. & Oster, G. F. (1993) *Biophys. J*. **65,** 316–324.
26. Englmeier, L., Fornerod, M., Bischoff, F. R., Petosa, C., Mattaj, I. W. & Kutay, U. (2001) *EMBO Rep*. **2,** 926–932.
27. Lindsay, M. E., Holaska, J. M., Welch, K., Paschal, B. M. & Macara, I. G. (2001) *J. Cell Biol.* **153,** 1391–1402.
28. Gitterman, M. & Weiss, G. H. (1994) *Chem. Phys*. **180,** 319–328.
29. Ribbeck, K. & Gorlich, D. (2002) *EMBO J.* **21,** 2664–2671.
30. Askjaer, P., Bachi, A., Wilm, M., Bischoff, F. R., Weeks, D. L., Ogniewski, V., Ohno, M., Niehrs, C., Kjems, J., Mattaj, I. W. & Fornerod, M. (1999) *Mol. Cell. Biol.* **19,** 6276–6285.
31. Bischoff, F. R. & Ponstingl, H. (1995) *Methods Enzymol.* **257,** 135–144.
32. Krupka, R. M. (1999) *J. Membr. Biol*. **167,** 35–41.
33. Kawasaki-Nishi, S., Nishi, T. & Forgac, M. (2001) *J. Biol. Chem.* **276,** 17941–17948.
34. Gnaiger, E., Mendez, G. & Hand, S. C. (2000) *Proc. Natl. Acad. Sci. USA* **97,** 11080–11085.
35. Sumbilla, C., Lewis, D., Hammerschmidt, T. & Inesi, G. (2002) *J. Biol. Chem.* **277,** 13900–13906.
36. Shah, S., Tugendreich, S. & Forbes, D. (1998) *J. Cell Biol.* **141,** 31–49.
37. Fornerod, M., van Deursen, J., van Baal, S., Reynolds, A., Davis, D., Murti, K. G., Fransen, J. & Grosveld, G. (1997) *EMBO J.* **16,** 807–816.
38. Kuersten, S., Arts, G. J., Walther, T. C., Englmeier, L. & Mattaj, I. W. (2002) *Mol. Cell. Biol.* **22,** 5708–5720.
39. Allen, N. P., Huang, L., Burlingame, A. & Rexach, M. (2001) *J. Biol. Chem.* **276,** 29268–29274.
40. Walther, T. C., Fornerod, M., Pickersgill, H., Goldberg, M., Allen, T. D. & Mattaj, I. W. (2001) *EMBO J.* **20,** 5703–5714.
41. Ishii, K., Arib, G., Lin, C., Van Houwe, G. & Laemmli, U. K. (2002) *Cell* **109,** 551–562.
42. Ferrell, J. E., Jr. (1998) *Trends Biochem. Sci*. **23,** 461–465.
43. Kaffman, A. & O'Shea, E. K. (1999) *Annu. Rev. Cell Dev. Biol.* **15,** 291–339.